Ice Motion Over Lake Vostok

R. Kwok[1], M. J. Siegert[2], and F. D. Carsey[1]

[1]*Jet Propulsion Laboratory*
California Institute of Technology
4800 Oak Grove Dr
Pasadena, CA 91109
USA

[2]*Bristol Glaciology Center*
School of Geographical Sciences
University of Bristol
Bristol, BS8 1SS
UK

Submitted to J. Glaciology
October, 1999

Ice Motion over Lake Vostok

R. Kwok, M. J. Siegert, and F. D. Carsey

Abstract

Ice motion over Lake Vostok is measured using repeat-pass Synthetic Aperture Radar (SAR) interferometry. The coverage of the lake and the components of the vector field are resolved using ten overlapping data takes from ascending and descending look directions. Seventy-day temporal baselines provide the sensitivity required to observe the range of ice motion (0-6 m/yr) over the lake and the adjacent ice sheet. It is remarkable that the scattering field remained coherent over these time separations. This is critical for interferometric analysis and can be attributed to the low surface accumulation and low air temperature at this elevation. The regional flow of the ice sheet around Lake Vostok is from West to East, perpendicular to the surface elevation contours. As the ice flows pass the grounding line, a southward component of motion that is correlated with the North-South surface slope along the length of the lake. The motion profile increases slowly from the northern tip of the lake and then more rapidly south of 77°S. At Vostok Station, the ice motion is 4.2 m/yr. Across the lake and away from the boundary effects, the down-lake flow pattern takes on parabolic profile with maximum velocity close to the center line of the lake. The overall influence of the subglacial lake is the addition of a down-lake motion component to the prevailing west-east motion of the ice sheet. As a result, we estimate 10% of the mass flowing onto the lake is diverted south. Reconstruction of the origins of the Vostok ice core indicates that it was grounded upglacier approximately 5000 years ago. This suggest a minimum freezing rate of 4 cm/yr for the subglacial accretion ice, ten times greater than that inferred from thermodynamic modeling of the upper 2 km of the ice core.

Introduction

Although Antarctic subglacial lakes were discovered over 20 years ago (e.g. Robin and others, 1977), the effect they have on overlying ice-sheet dynamics has yet to be quantified. The largest subglacial lake is located beneath Vostok Station, central East Antarctica (Kapitsa and others, 1996; Siegert and Ridley, 1998). ERS-1 satellite altimetry indicates that an unusually smooth, flat feature exists within the ice-sheet surface above Lake Vostok. This morphology is caused by changes in the dynamics of ice that is grounded compared with floating ice over subglacial lakes. Since shear stress across the ice-water boundary above subglacial lakes is effectively zero, the ice sheet must flow over the lake by a mechanism (probably longitudinal extension) similar to that in ice shelves, rather than by the base-parallel shear deformation that occurs in cold-based grounded ice. Consequently, the dynamic characteristics of the ice sheet will be altered as ice flows across the margin of the lake, as the basal shear stress is reduced to zero. The aim of this paper is to measure the ice velocity field over Lake Vostok from interferometric SAR (InSAR) data. The effects of the subglacial lake on the large-scale motion field on ice sheet mass balance, bottom ablation/accretion and the origins of the Vostok ice core are briefly discussed.

Glaciological Setting

The aerial extent of the Vostok subglacial lake can be estimated from two geophysical datasets (1) airborne radar which supplies information from the ice-sheet base and (2) satellite altimetry (from, for instance, the ERS-1 satellite) of the flat region on the ice-sheet surface above the subglacial lake (Siegert and Ridley, 1998).

There is a very strong correlation between the airborne radar-determined location of Lake Vostok (Robin and others, 1977; Ridley and others, 1993; Kapitsa and others, 1996) and the position of the anomalous flat-surfaced region of the ice sheet above the lake (Siegert

and Ridley, 1998). The margin of the flat surface region matches so well with the radar-observed edge of the lake, that the lake extent can be been mapped accurately from the satellite altimetry (Kapitsa and others, 1996).

Lake Vostok is 230 km long, and up to 50 km wide, with a surface area of ~14,000 km^2 making it one of the world's largest lakes. Satellite radar altimetry shows that the ice sheet above Lake Vostok has an approximately north-south surface slope of 0.004° (0.25 m km^{-1}). The ice-sheet surface thus drops by about 40 m across the 230 km length of the lake. The relatively flat ice-sheet surface over Lake Vostok contrasts with the surface slope of the surrounding ice sheet. Both to the east and west of the lake, the surface slope of the grounded ice sheet is relatively uniform at approximately 0.08° (1.4 m km^{-1}). The general direction of grounded ice-flow, assumed to be parallel to the surface slope, alters from north-eastward around the northern end of Lake Vostok, to eastward near to the south of the lake (Siegert and Ridley, 1998). A few kilometres east of, and along the 200-km-long western margin of the lake, lies a small (~2 m) trough in the ice-sheet surface, about 10 km wide. Also, a few kilometres east of the eastern margin of the lake, a small topographic rise occurs, ~5 m high, ~10 km wide, and over 200 km in length.

Through analysis of the airborne radar data, the ice thickness over Lake Vostok and the subglacial topography have been measured (Siegert and Ridley, 1998). Ice thickness is more than 4200 m over the northern region of the lake and thins steadily along the length of the lake such that, beneath Vostok Station, it is 3740 m. The height of the lake surface at its northern end is around -700 m above sea level. This elevation increases toward the south of the lake where, beneath Vostok Station, the surface elevation of the lake is at around -300 m. The north-south subglacial gradient at the ice-lake interface is around 10 times greater than, and in the opposite direction to, the surface slope of the ice sheet.

Lake Vostok is located within a subglacial topographic basin, the topographic setting of which is characteristic of a rift-valley. The basin has a crescentic shape, and the side walls are relatively steep (with gradients up to 0.1) and high (up to 1000 m above the surface of the lake). When one considers that Lake Vostok is 500 m deep in the south and may have several hundred metres of glacial sediments over its floor (Kapitsa and others, 1996), the subglacial valley may be as much as 2000 m deep and 5000 m below the surface of the ice sheet.

The Ice Motion Field

ERS tandem mission data set

The ERS-1 SAR data used here were acquired during the ERS tandem mission. The data from the ERS-1 and ERS-2 radars acquired over the region around Lake Vostok, were captured at the McMurdo Reception Facility and shipped to the Alaska SAR Facility (ASF) for archive and distribution. The 10 SAR datatakes, containing 42 frames of SAR data, used were provided by ASF. The details of the data set are shown in Table 1. The SAR image mosaics of the ascending and descending datatakes used in the motion analysis are shown in Fig. 1.

Repeat-pass interferometry

We construct the flow field with motion observations from repeat-pass interferometry acquired during the ascending and descending data takes. For background discussions on the theory and techniques for derivation of glacial motion and topography using repeat-pass interferometry, the reader is referred to articles in the published literature (Goldstein and others, 1993; Kwok and Fahnestock, 1996; Joughin an others, 1998). We present a brief review here. The interferometric phase of a given sample can be expressed as the sum of topography and displacement-dependent terms,

$$\phi = \phi_{topography} + \phi_{displacement}$$

The first term, $\phi_{topography}$, contains phase variations from surface relief; the sensitivity of which is directly proportional to the length of the interferometric baseline. If the surface is displaced along the radar line-of-sight between repeat observations, then the observed phase includes a second phase contribution, $\phi_{displacement}$, where

$$\phi_{displacement} = \frac{4\pi}{\lambda} v_p \Delta T \sin\theta.$$

λ is the radar wavelength, $v_p \Delta T$ is the surface motion, θ is the incidence angle, and ΔT is the time separation between observations. v_p represents the component of surface velocity in the radar look direction. This term is independent of the spatial baseline and is dependent on only the temporal baseline, ΔT. Available temporal baselines from the ERS tandem mission are 1, 35, and 70 days. For these baselines, a 2π radian (1 fringe) change in $\phi_{displacement}$ is equivalent to a change in velocity (v) of 26.1 m/yr, 0.75 m/yr, and 0.37 m/yr, respectively. For the magnitude of velocities (0-6 m/yr) we expect to find around Lake Vostok, the 70-day temporal baseline provides the maximum sensitivity to small variations in the motion field and this is what we use in the following analysis.

Target Coherence

Typically, the use of long temporal baselines to detect surface motion is limited by the coherence of the target scattering field over the time separation. If scattering properties are altered by precipitation or other physical processes, then coherence would be reduced or destroyed. Table 1 shows the coherence of 25 km by 25 km sample regions on the lake surface for all the interferometric pairs used our analysis. We note that the repeat-pass interferograms used here have the longest temporal baselines ever attempted for detection of ice motion. Modest coherence is maintained for all the data take pairs. We attribute this to the below freezing temperatures and low accumulation rate (~3 cm/yr) at this elevation on the ice sheet. A dependence of the coherence on the perpendicular baseline length, $B_\perp$, is evident. The highest coherence is exhibited by the samples from the data take pair with the shortest baseline while the lowest coherence is exhibited by the samples form the pair

with the longest baseline. $B_\perp$ is the component of the baseline perpendicular to the radar look direction and is a measure of the angular separation between the observation points. Decorrelation due to perpendicular baseline separation well below the critical baseline (~1 km for ERS) is believed to be dependent on the vertical extent of the scattering medium. Indeed, for volume scattering media like snow and glacial ice, this dependence has been used to estimate the penetration depth of the radio waves into the scattering volume (Hoen and Zebker, 1999).

Estimation of the 2-D motion fields

The 1-D motion estimates from individual ascending and descending data takes are produced by first removing the topographic contribution, $\phi_{topography}$, to the interferometric phase. $\phi_{topography}$, is simulated using a Digital Elevation Model (DEM) derived from ERS altimetry and the interferometric baselines (provided by Dr J. Bamber). The motion only phase field, $\phi_{displacement}$, is then ϕ - $\phi_{topography}$.

To construct the velocity field from ascending and descending data takes, we follow the procedure described in Joughin an others (1998). In general, the velocity vector consists of three components (v_x, v_y, v_z). For motion tangent to the ice surface, the phase can be written as,

$$\phi_{displacement} = \frac{4\pi}{\lambda}\Delta T(v_p \sin\theta - v_z \cos\theta)$$

where v_p is the motion projected onto a plane tangent to the surface of the ellipsoid. v_x and v_y are defined on the tangent plane and v_z is the vertical motion. The magnitude of v_z is approximately,

$$v_z \sim v_p \frac{\partial z}{\partial x}$$

With the surface slope ($\partial z/\partial x$) around Lake Vostok to be approximately 0.08° (and θ= 23°) and v_p ~3 m/yr, the projection of v_z onto the range look direction ($v_z \cos\theta$ ~0.004

m/yr) contributes less than 0.2 radians to the interferometric phase. For our analysis here, we ignore the contribution of this insignificant term.

Using this assumption, the ascending and descending data takes each provide an observation of the total velocity vector, $\boldsymbol{v}$,

$$v_a = \boldsymbol{v} \cdot \boldsymbol{a}$$
$$v_d = \boldsymbol{v} \cdot \boldsymbol{d}$$

where v_a and v_d are the 1-D velocities derived from interferometry and $\boldsymbol{a}$ and $\boldsymbol{d}$ are the unit vectors defining the direction of the range vectors on the tangent plane described above. Rewriting the above equation in matrix notation gives,

$$\begin{pmatrix} v_a \\ v_d \end{pmatrix} = \begin{pmatrix} a_x & a_y \\ d_x & dy \end{pmatrix} \begin{pmatrix} v_x \\ v_y \end{pmatrix}$$

The orthogonal components of velocity field can thus be solved viz.,

$$\begin{pmatrix} v_x \\ v_y \end{pmatrix} = \begin{pmatrix} a_x & a_y \\ d_x & dy \end{pmatrix}^{-1} \begin{pmatrix} v_a \\ v_d \end{pmatrix}$$

Error Analysis

There are three primary sources of error in the motion estimates:

1. Errors due to uncertainty in the spatial baselines.
2. Effect of unaccounted topography (surface relief features which are not resolved in altimeter DEM).
3. Use of a stationary point on Ridge B as a velocity tiepoint.

In the absence of velocity tiepoints for refining the baseline estimates, we use the precise ERS orbits to determine the interferometric baselines. The radial errors of individual precision orbits are estimated to be approximately 5 cm (Scharroo and Visser, 1997). The effect of this baseline uncertainty is the introduction of residual linear phase ramps in the range direction due to the incomplete removal of the topographic phase term, $\phi_{topography}$,

which is dependent on the spatial baseline. In our analysis, this residual phase would be interpreted incorrectly as target motion. Simulation shows that a 7 cm ($\sqrt{2} \times 5$ cm) uncertainty in baseline would introduce a maximum phase bias of approximately $\pi/2$ radians (0.25 fringe), or an error of approximately 0.1 m/yr (or 0.37/4 m/yr). This is probably the best-case error. In reality, we expect an error somewhat worse as errors propagate when several data takes are mosaicked together. This mosaic-induced is by far the largest source of uncertainty in our motion estimates.

There are surface relief variations in the high-resolution SAR data that are not present in the lower resolution altimeter DEM. These residuals affect only the small length scale motion because the large scale DEM is essentially unbiased over relatively smooth terrain. The magnitude of these residuals is dependent on the length of the baseline, especially perpendicular component $B_{\perp}$, because larger baseline interferometers are more sensitive to topographic variations. Since surface slopes are relatively small on the ice sheet, especially over the lake, we do not expect this to be a large source of error in our motion estimates. Figs. 2 and 3 show the corresponding one-dimensional motion fields derived from ascending and descending passes. Artifacts due to small scale topography can be seen as rumples in the motion field. These are especially obvious in the motion mosaics when adjacent data takes have very different baselines. For example, the third data take from the right in Fig. 2a has a much smaller baseline than its neighbors thus causing a visible seam in the mosaic.

InSAR measurements provide only relative motion observations. A point on the Ridge B ice divide is selected as the point of no motion (see location on Fig. 2) to tie down the motion estimates. Both ascending and descending motion mosaics were referenced to this point. We compare our motion estimate with the only direct measurement of the surface velocity that was made within 20 km of Vostok station in 1964 and 1972 (Liebert and Leonhardt, 1974), approximately 280 km away. The astronomical measurements, from

star sights, give a velocity of 3.7±0.7 m/yr at 142±10° relative to true north. Our estimates give a velocity of 4.2 m/yr at 130° relative to true north, close to the expected uncertainty in our estimates.

Results and Discussion

Motion Field

The derived 2-D motion field at the overlap between the ascending and descending passes are shown in Figs. 4a and 4b. The field is shown as a vector map and velocity contours.

The Lake is situated approximately 280 km east of Ridge B. The regional ice dynamics around the lake are controlled by local surface slopes. The velocities west of the lake are small, as the ice flow away from the ice divide. The motion ranges from 0 m/yr near the ice divide to around 3 m/yr on the western margin of the lake. The derived motion vectors are close to perpendicular to the elevation contours. There is an absence of crevassing along the boundaries of the lake and there is a lack of visible flow lines or lineations in the SAR imagery probably due to the relatively slow motion and high strength of the very cold ice (Fig. 1).

The influence of the lake on ice motion can be seen in the velocity fields and the velocity contours. Because of the close alignment of the radar look direction relative to the long axis of the lake, the ice motion along the lake is clearest in the 1-D flow field derived from the ascending passes (Fig. 2a). A visible southward component of motion can be observed as the ice flows across the western margin. The boundaries of the lake can be easily delineated by the changes in this motion field. Along the 280 km length of the lake, the surface elevation drops by almost 25 m on the southern half of the lake (south of 77°S) compared to an elevation change of only 10-15 m on the northern half (see elevation contours in Fig. 3). The increases in surface velocity are well-correlated to increases in the surface slope of the lake; the ice motion is slower on the northern half of the lake

compared to the southern half. The velocity varies between 2 m/yr to 4.5 m/yr in the southern half, and the velocity gradients (Fig. 4) are highest near Vostok Station. The increase in the southward component is highly correlated to the surface slope of the lake. Away from the lake boundaries effects, the across-lake flow pattern (in the southern half) takes on parabolic profile with maximum velocity close to the center-line of the lake. Absence of basal drag allows ice flow to respond quickly to small changes in surface slopes.

In the east-west direction, the surface of the ice is relatively flat with less than several meters of drop in elevation between the lake margins. The across-lake motion prevails – the ice motion does not flow perpendicular to the surface slopes. The flow slows as the ice sheet re-grounds on the eastern margin. East of eastern lake boundary, the derived flow pattern is again close to perpendicular to the elevation contours. Overall, the presence of the lake adds a southward component to the west-east flow of the ice sheet.

Mass Balance

Due to the influence of the lake, a certain volume of the ice is diverted southward although not as significant as if all the ice had to flow through the southern lakeshore. Mean flow velocities of 2-3 m/yr across the 280 km wide, 3.5 km thick western margin results in a flux of 3.0×10^9 m^3/yr. If we assume that the southern boundary to be 25 km wide, using the motion profile the southward mass flux would be approximately 3.0×10^8 m^3/yr.The southward component due to the influence of the lake diverts approximately 10% of the mass in this direction.

Origin of the Vostok Ice Core

Assuming a steady-state motion field, we can construct motion trajectories to determine the approximate origins of ice particles on the lake. Fig. 5 shows several trajectories, including one with a termination point at Vostok Station, created by back propagation of

the flow field. The trajectory shows that the ice core at the present day location of Vostok Station was grounded less that 5000 years ago. This has certain implications concerning the thermal and mechanical processes of the accretion ice near the bottom of the lake ice.

Recent analysis of heat flow and internal deformational heating (Salamatin and others, 1998) results in subglacial (lake ice) growth rates between 1 and 4 mm per year, depending on the level of strain heating from shear between moving and stationary ice. The entire layer of accretion ice is 220 m thick, but this ice is actually two strata, one containing visible mineralogic inclusions above a cleaner layer characterized by very large crystals (Petit and others, 1999; Lipenkov and Barkov, 1998; and Petit, 1999). If all the accretion ice is from Lake Vostok, the time implied for passage over water is 55 to 220 kyr. If only the clean ice strata is from the lake the time over water ranges from 140 to 35 kyr. In either case the joint growth rate and thickness lead to an inference that the ice on which the Vostok Station rests had been in accretion for about 10 times longer than the velocity data indicate possible. This is too large to be accommodated in the growth rate uncertainty, which is well established, and it is unlikely that the ice motion changed dramatically over the past 5000 years. The ice motion suggests a freezing rate of approximately 4 cm/yr.

It is possible that the ice strata characterized by mineralogic inclusions was accreted from upglacier of the lake. This does not solve the problem, but it is worth examination. The consequence of this accretion is that the ice sheet upglacier of Lake Vostok is below the local freezing point, and this is highly unlikely. In fact, additional small subglacial lakes have been noted upglacier in both sounding radar (Siegert and others, 1998; Dowdeswell and Siegert, 1999) and satellite altimeter maps (Bamber and Bindschadler, 1997).

Summary

The motion field over Lake Vostok is measured using repeat-pass SAR interferometry with a relatively long temporal baseline of 70 days. The 2-D vector field is resolved using observations from ascending and descending look directions. The regional flow of glacial ice surrounding Lake Vostok is controlled by the west-east surface slopes of the ice sheet. Over the lake, measurements show that there is an observable southward component of motion which can be explained by surface slopes along the length of the lake and the absence of basal drag. The prevailing east-west flow of the ice sheet motion is modified by this southward motion. Specifically, the ice sheet velocity over the lake is greatest near Vostok Station (4.2 m/yr) and is slowest toward the northern end of the lake, where ice velocity is less than 1 m/yr. Between the lake boundaries, the southward velocity profile exhibits a parabolic profile. The ice velocity field allows us to reconstruct ice flowlines across the lake. The line crossing the Vostok ice core site shows that the ice within the core could have been grounded upstream of Lake Vostok about 5000 years ago. Since 200 m of ice have been accreted to the underside of the ice sheet from the lake, we attribute a minimum freezing rate of around 4 cm/yr, ten times greater than that inferred from thermodynamic modeling of the upper 2 km of the ice core.

Acknowledgments

We wish to thank Dr. J. L. Bamber, University of Bristol, for providing the DEM of Antarctica for our study. R. Kwok and F. D. Carsey performed this work at the Jet Propulsion Laboratory, California Institute of Technology under contract with the National Aeronautics and Space Administration.

References

Bamber, J. L. and R. Bindschadler, An improved elevation dataset for climate and ice-sheet modelling: validation with satellite imagery, *Ann. Glacio.*, 25, 439-444, 1997.

Dowdeswell, J.A., and Siegert, M.J., The dimensions and topographic setting of Antarctic subglacial lakes and implications for large-scale water storage beneath continental ice sheets. *Geological Society of America Bulletin*, 111, 254-263, 1999.

Goldstein R. M., H. Engelhardt, B. Kamb, R. M. Frolich, Satellite radar interferometry for monitoring ice sheet motion: Application to an Antarctic Ice Stream, *Science*, 262, 1525-1530, 1993.

Hoen, E. W. and H. A. Zebker, Penetration depth inferred from interferometric volume decorrelation observed over the Greenland ice sheet, *Proceedings of IGARSS*, Hamburg, Germany, 1999.

Kapitsa, A. P., J. K. Ridley, G. de Q. Robin, M. J. Siegert and I. A. Zotikov, A large deep freshwater lake beneath the ice of central East Antarctica, *Nature*, 381, 684-686 (1996).

Kwok, R. and M. Fahnestock, Ice sheet motion and topography from radar interferometry, *IEEE Trans. Geosci. Remote Sens.* 34(1), 189-200, 1996.

Liebert, J. and G. Leonhardt, Astronomic observations for determining ice movement in the Vostok Station area, *Inf. Bull. Sov. Antarct. Exped.*, 88, 68-70, 1974.

Lipenkov, V. and N. Barkov, Internal structure of the Antarctic ice sheet as revealed by deep core drilling at Vostok Station, in Lake Vostok Study: Scientific objectives and technological reauirements, international workshop, Arctic and Antarctic Research Institute, St Peteresburg, Russia, 1998.

Joughin, I., R. Kwok, and M. Fahnestock, Interferometric Estimation of three-dimensional ice-flow using ascending and descending passes, 36(1), 25-37, 1998.

Petit, J. R., Evidence from the Vostok ice core studies, in Bell and Karl, eds. Lake Vostok Workshop Final Report, 1999.

Petit J.R., J. Jouzel, D. Raynaud, N. I. Barkov, J. M. Barnola, I. Basile, M. Bender, J. Chappellaz, M. Davis, G. Delaygue, M. Delmotte, V. M. Kotlyakov, M. Legrand, V. Y. Lipenkov, C. Lorius, L. Pepin, C. Ritz, E. Saltzman, M. Stievenard, Climate and atmospheric history of the past 420,000 years from the Vostok ice core, Antarctica *Nature*, 399: (6735) 429-436, 1999.

Ridley, J. K., W. Cudlip, and S. W. Laxon, Identification of sub-glacial lakes using ERS-1 radar altimeter, *J. Glacio.*, 39, 625-634, 1993.

Robin, G. de Q., D. J. Drewy, and D. T. Meldrum, International studies of ice sheet and bedrock, *Phil. Trans. R.Soc. London*, 279, 185-196, 1977.

Salamatin, A., R. Vostretsov, J. Petit, V. Lipenkov, and N. Barkov, Geoophysical and paleoclatimatic implications of the stacked temperature profile from the deep borehole at Vostok Station (Antarctica), Materialy Glyatsiologicheskikh Isslefovanii, 85, 233-240, 1998.

Scharroo, R., and P. N. A. M. Visser, ERS Tandem Mission orbits: is 5 cm still a challenge? *Proceedings of the Third ERS Symposium*, Florence, 17-21 March 1997, ESA SP-414.

Siegert, M. and J. K. Ridley, An analysis of the ice-sheet and subsurface topography above Vostok Station subglacial lake, central East Antarctica, *J. Glacio.*, 103(B5), 10195-10207, 1998.

Siegert, M.J., Dowdeswell, J.A., Gorman, M.R., and McIntyre, N.F., An inventory of Antarctic subglacial lakes. *Antarctic Science*, 8, 281-286, 1996.

Figure Captions

Figure 1. ERS-1 SAR image mosaics of Lake Vostok. (a) Ascending datatakes. (b) Descending datatakes. The image maps are presented on a polar stereographic projection centered at the South Pole, with the map vertical defined by the Greenwich meridian. The dimensions of the images are 463 km by 505 km. (ERS-1 images ©ESA 1999)

Figure 2. 1-D motion field derived from ascending and descending repeat-pass interferometry. These are radar line-of-sight motion projected onto the plane tangent to the local ellipsoid. The approximate radar look direction is indicated by the arrow. The motion is referenced to a stationary point (indicated by an X) on the Ridge B ice divide.

Figure 3. 2-D vector field computed at the overlap between the ascending and descending datatakes. The vector field is overlaid on the image mosaic constructed from ascending passes. Elevation contours are also shown. Contour interval of the black and white contours are 25 m and 10 m, respectively.

Figure 4. Velocity contours of the 2-D vector field computed at the overlap between the ascending and descending datatakes The velocity contours are overlaid on the image mosaic constructed from ascending passes.

Figure 5. 100,000-yr trajectories showing the origins of ice parcels on the ice sheet. The time interval between filled circles along the path is 5000 years.

Table 1
ERS-1 repeat-pass datatakes, their baselines, and
on-lake coherence between the interferometric pairs

Datatake/Date		Datatake/Date		Asc/Dsc	$B_\perp$	$B_\parallel$	Correlation (on Lake)
23993	15-Feb-96	24995	25-Apr-96	A	61.97	-59.75	0.41±0.09
23793	1-Feb-96	24795	11-Apr-96	A	-61.32	-95.82	0.42±0.09
23965	13-Feb-96	24967	23-Apr-96	A	96.10	-38.93	0.31±0.12
23765	30-Jan-96	24767	9-Apr-96	A	-104.40	-112.36	0.32±0.09
23894	8-Feb-96	24896	18-Apr-96	A	240.72	16.53	0.23±0.09
23980	15-Feb-96	24982	25-Apr-96	A	88.62	-41.92	0.31±0.10
23935	11-Feb-96	24937	21-Apr-96	D	129.25	-26.24	0.35±0.09
23949	12-Feb-96	24951	22-Apr-96	D	83.36	-44.85	see note[3]
23820	3-Feb-96	24822	13-Apr-96	D	15.90	-68.09	0.50±0.08
23777	31-Jan-96	24779	10-Apr-96	D	-113.34	-115.69	0.32±0.09

Notes:
1. All interferometric pairs have 70-day temporal baselines.
2. Correlation coefficients are computed within the lake boundaries over an area of 25 km by 25 km.
3. The correlation coefficient was not computed for pair 23949/24951 because these datatakes do not contain the lake.

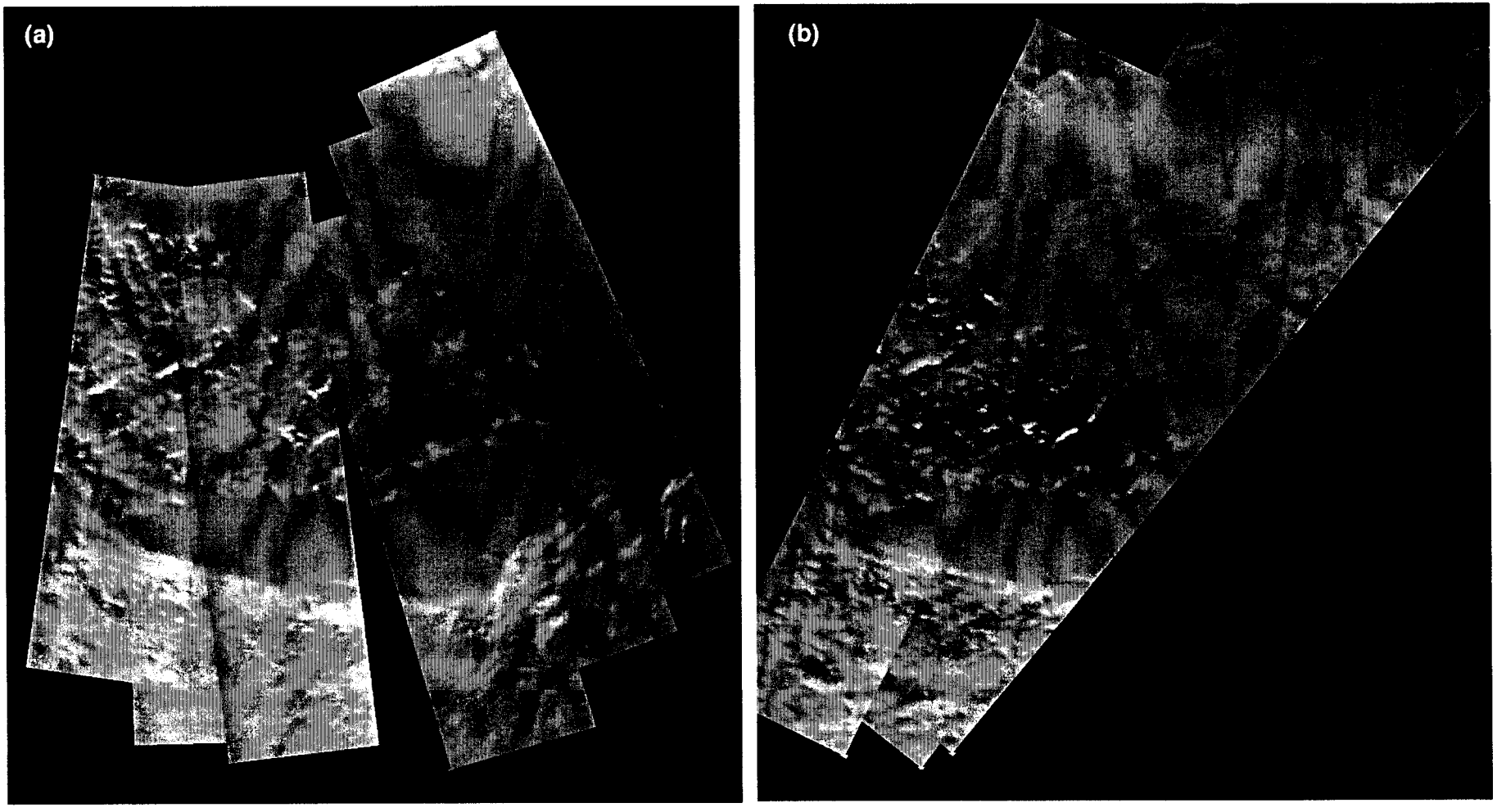

Figure 1

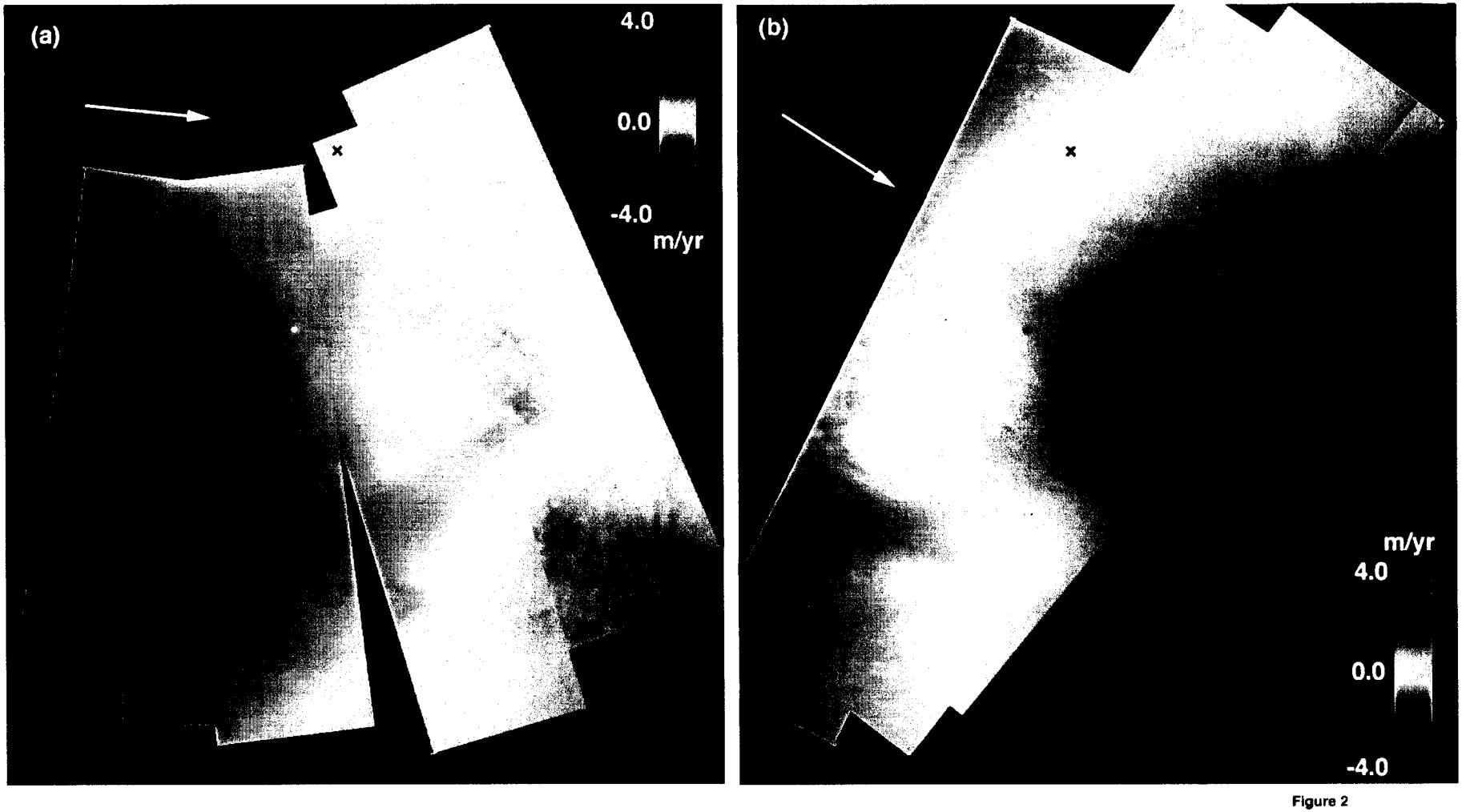

Figure 2

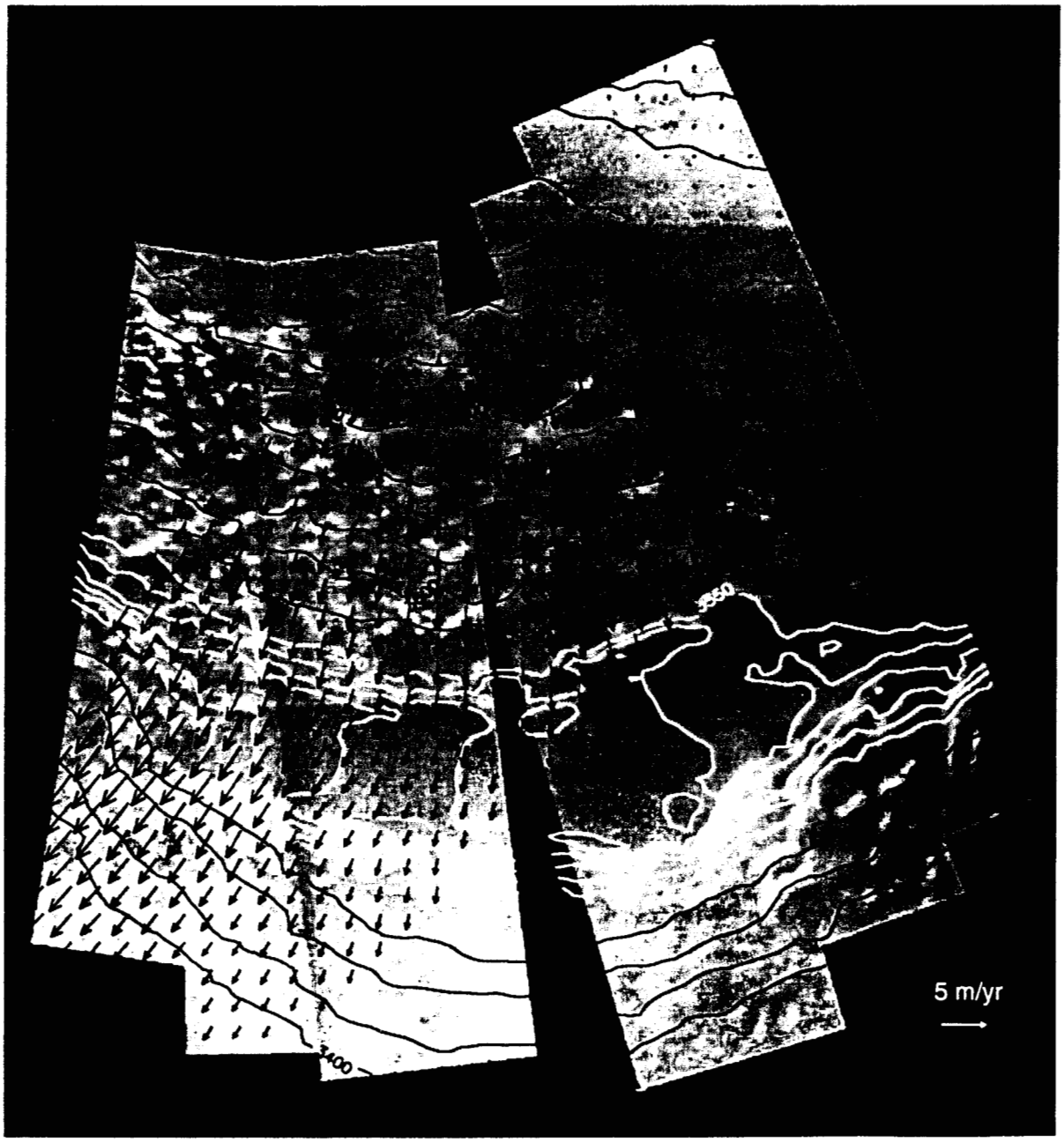

Figure 3

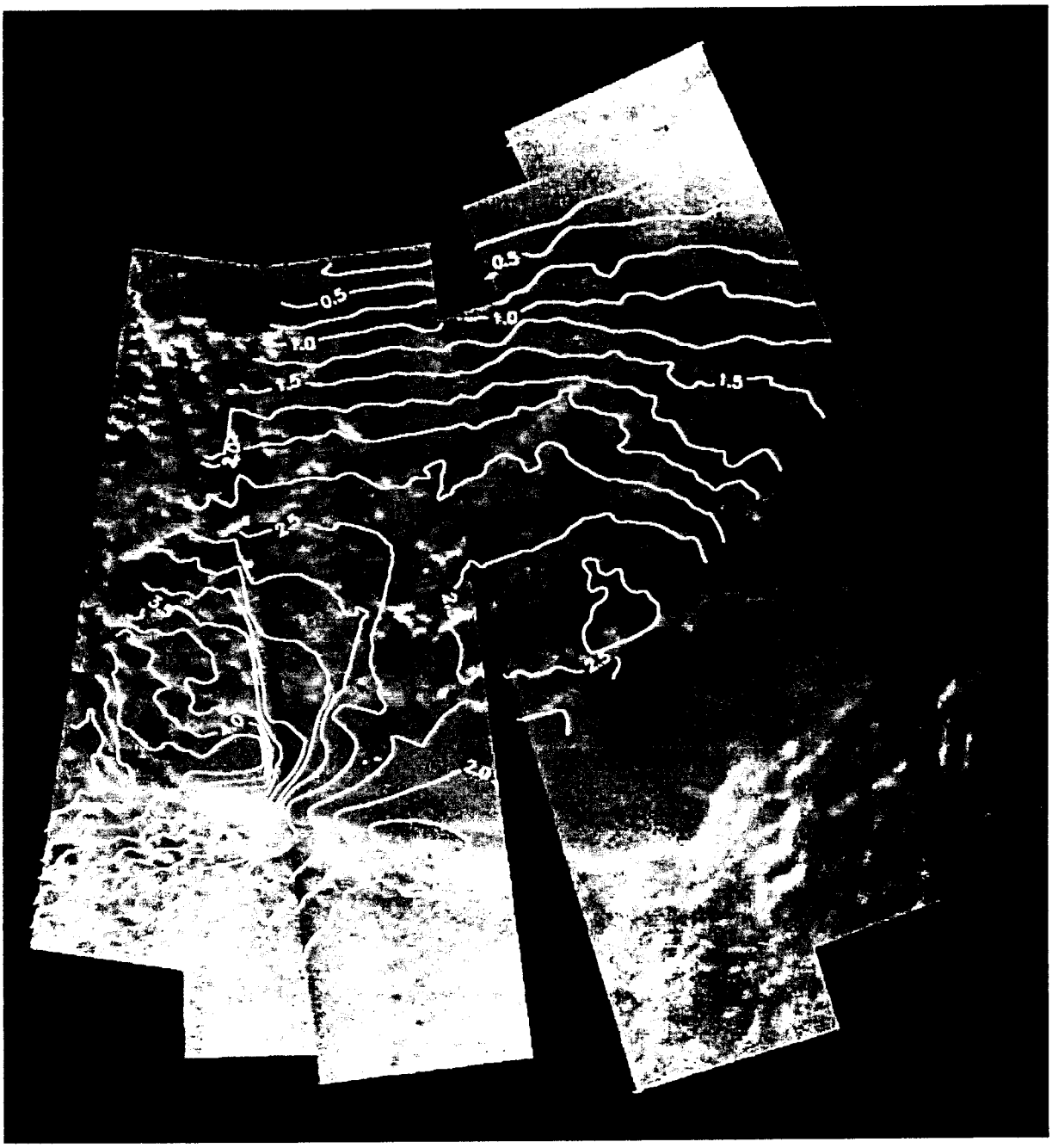

Figure 4

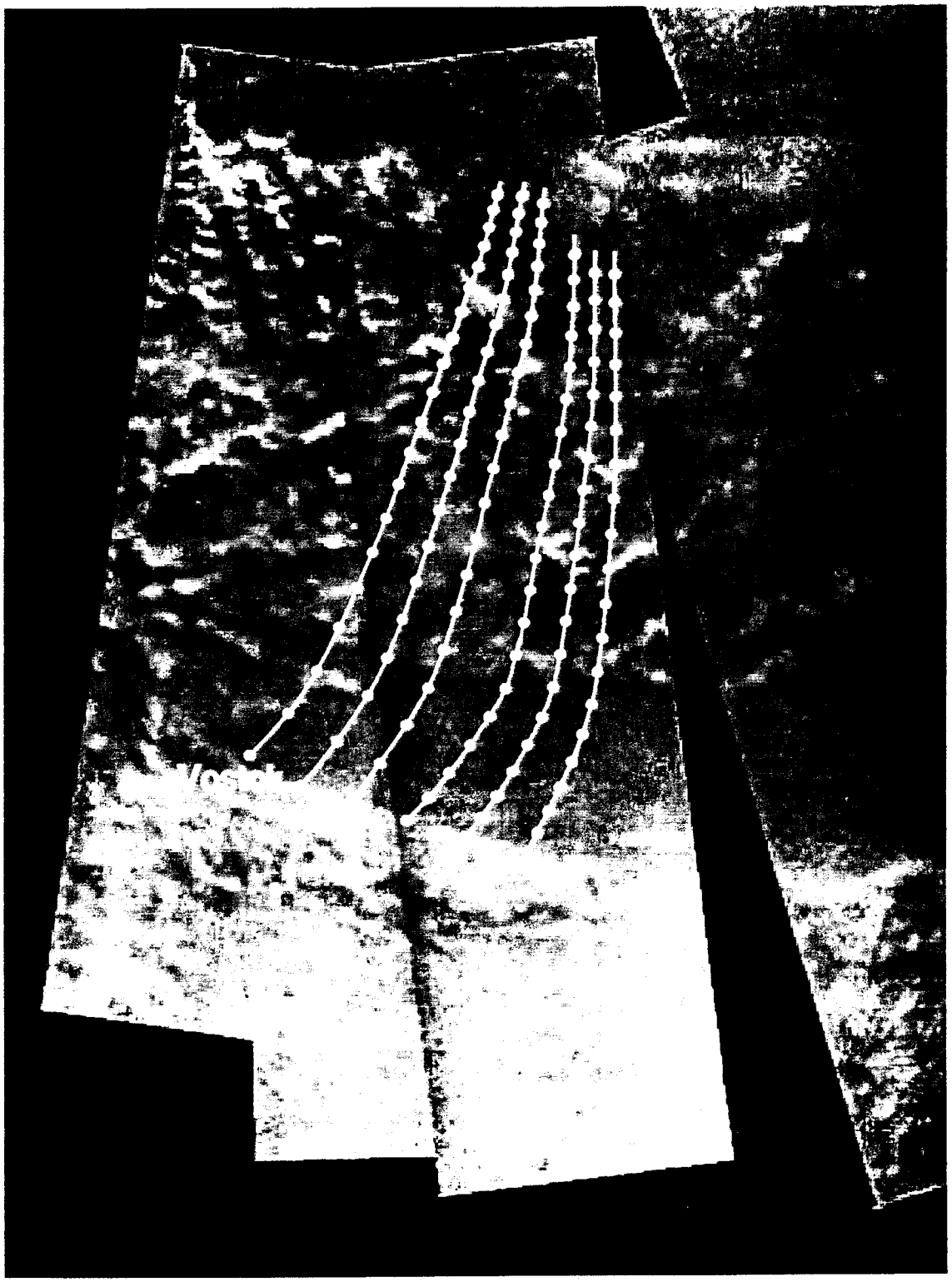

Figure 5